

Amorphous precursors of crystallization during spinodal decomposition

Leopoldo R. Gómez^{1,2,*} and Daniel A. Vega¹

¹*Department of Physics and Instituto de Física del Sur, IFISUR (UNS-CONICET), Alem 1253, (8000) Bahía Blanca, Argentina*

²*Instituut-Lorentz, Universiteit Leiden, P.O. Box 9506, NE-2300 RA Leiden, The Netherlands*

(Received 4 July 2010; revised manuscript received 18 December 2010; published 10 February 2011)

A general Landau's free energy functional is used to study the dynamics of crystallization during liquid-solid spinodal decomposition (SD). The strong length scale selectivity imposed during the early stage of SD induces the appearance of small precursors for crystallization with icosahedral order. These precursors grow in densely packed clusters of tetrahedra through the addition of new particles. As the average size of the amorphous nuclei becomes large enough to reduce geometric frustration, crystalline particles with a body-centered cubic symmetry heterogeneously nucleate on the growing clusters. The volume fraction of the crystalline phase is strongly dependent on the depth of quench. At deep quenches, the SD mechanism produces amorphous structures arranged in dense polytetrahedral aggregates.

DOI: [10.1103/PhysRevE.83.021501](https://doi.org/10.1103/PhysRevE.83.021501)

PACS number(s): 64.70.dg, 64.70.dm, 64.60.Bd, 61.43.—j

I. INTRODUCTION

According to the classical theory of symmetry-breaking phase transitions, the crystallization process may proceed via two distinct mechanisms, nucleation and growth (NG) or spinodal decomposition (SD) [1]. In the NG mechanism the initial disordered phase is metastable, and the relaxation of the system is promoted by the overcoming of a free energy barrier. This process involves the formation of a critical nucleus of the crystalline phase by structural fluctuations. In a manner different from the NG process, SD does not require large fluctuations to initiate the phase transition, and it is characterized by the exponential growth of density fluctuations of a dominating wavelength, entirely determined by the thermodynamic properties of the system. At early times this process leads to the formation of disordered isotropic states that eventually evolve toward the equilibrium phase through coarsening [2,3].

Although this classical picture provides a qualitative description of the phenomenology involved in the phase transition process, during the last 30 years, experiments, theory, and simulations have shown that the process of crystallization is far from being trivial. For example, in the NG process, the kinetic pathway toward equilibrium may involve intermediate phases with a symmetry different than those corresponding to equilibrium [4–9]. According to Ostwald's step rule the nucleated phase is not necessarily the thermodynamically most stable, but it has energy levels closest to the disordered state [5]. A similar process was observed in the crystallization of globular proteins and colloids, where density inhomogeneities in the fluid lower the free energy barrier for NG [6–9]. On the other hand, the relaxation in the spinodal region is still poorly understood. For example, it has been recently observed that thermal fluctuations play an important role in the dynamics of SD. In the neighborhood of the spinodal line, it was found that the equilibrium phase can be pseudonucleated by density wave fluctuations [10]. A complex phase separation kinetics has been observed also in different systems, such as colloids

and polymers, where it has been found that a spinodal-like dynamics can precede the crystallization process [10,11].

In this work a continuous Landau's free energy expansion and a relaxational dynamics are used to study the kinetics of crystallization of a body-centered cubic (bcc) structure in the spinodal region. As compared with molecular dynamics simulations, the phase field approach employed here naturally incorporates the elasticity of the bcc crystals and provides an efficient approach over diffusive time scales, while the identification of the precursors of crystallization as well as amorphous and crystalline regions can be easily determined through the local amplitude of the continuum order parameter.

II. MODEL

Symmetry-breaking phase transitions in a wide variety of systems can be studied through an expansion of the free energy Φ in terms of an appropriated order parameter ψ . Here we employ the expansion [12]

$$\Phi = \int \left[W(\psi) + D(\nabla\psi)^2 + b \int \frac{\psi(\mathbf{r})\psi(\mathbf{r}')}{|\mathbf{r}-\mathbf{r}'|} dV' \right] dV, \quad (1)$$

where $W(\psi) = -\tau\psi^2 + \nu\psi^3 + \lambda\psi^4$. Here the order parameter represents the deviation of the particle density from the uniform value characteristic of the liquid state (where $\psi = 0$). The parameter τ is proportional to $T_S - T$, being a measurement of the depth of quench, with T_S the spinodal temperature where the continuous phase transition begins. The constants ν and λ are related to the symmetry and saturation of ψ at equilibrium, and D is a free energy penalization to the spatial variations of the order parameter [2,3,13].

The dynamics of SD can be studied through a Cahn-Hilliard equation [14]: $\partial\psi/\partial t = M\nabla^2(\delta\Phi/\delta\psi)$, where M is a mobility coefficient. By inserting the free energy functional [Eq. (1)] in the relaxational equation, the following equation for the evolution of the order parameter can be obtained:

$$\frac{\partial\psi}{\partial t} = M\nabla^2 \left[\frac{dW(\psi)}{d\psi} - D\nabla^2\psi \right] - M b \psi. \quad (2)$$

In this work Eq. (2) was numerically solved through finite-difference methods on cubic grids having 128^3 and 256^3 grid points using periodic boundary conditions. After

*gomez@lorentz.leidenuniv.nl

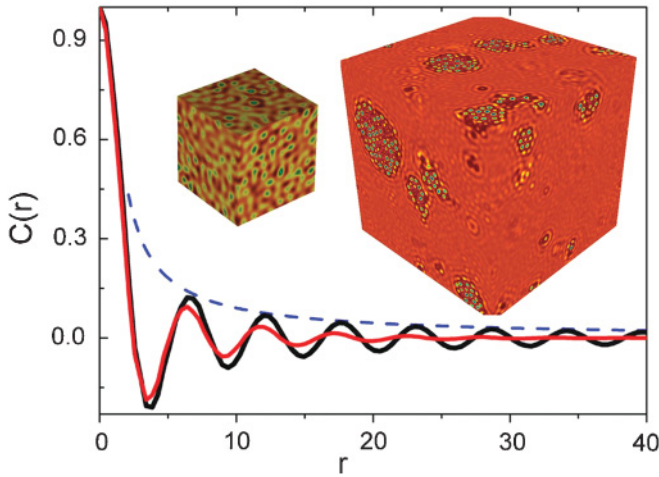


FIG. 1. (Color online) Early autocorrelation function $C(r)$ values for a system quenched into the spinodal region with reduced temperatures $\tau_r = (\tau - \tau_S)/\tau_S = 1 \times 10^{-5}$ (black line) and $\tau_r = 1 \times 10^{-1}$ [red (gray) line]. The dashed blue (dashed gray) line indicates $C(r) \sim 1/r$. The inset shows the early-time real space fluctuations (left) and the formation of precursors by the nonlinear enhancement of density fluctuations (right).

SD the systems contain around 1.0×10^5 particles. The initial homogeneous state is modeled by a random distribution of order parameter fluctuations [2,3].

III. RESULTS

Since the initial disordered state is characterized by small fluctuations ($\psi \sim 0$), the early dynamics is almost linear and the system's state can be described as a random superposition of density waves of the form [10] $\psi(\mathbf{r}, t) = \sum_{\mathbf{k}} A_{\mathbf{k}} \exp[i\mathbf{k} \cdot \mathbf{r} + \lambda(k)t]$. Here $A_{\mathbf{k}}$ is the initial amplitude of the \mathbf{k} mode and the amplification factor $\lambda(k) = -Dk^4 + \tau k^2 - b$ selects the range of unstable modes [those modes for which $\lambda(k) > 0$]. In real space the system displays a disordered pattern characterized by a dominating length scale related to the most unstable modes [10].

For systems quenched slightly below the spinodal line, where $\tau_S = 2\sqrt{bD}$, the region of unstable modes becomes sharply peaked around a dominating wave vector amplitude $k_0 \sim \sqrt{\tau/D}$. In this case the random superposition of modes leads to the emergence of a strongly correlated filamentary network of density wave fluctuations, with strong similarities to those found in quantum billiards and other physical phenomena involving random wave superposition [10]. Figure 1 shows the long-range density correlations that emerge in the early state. In this case, the azimuthally averaged two-point correlation function, $C(r) = \langle \int d\mathbf{r}' \psi(\mathbf{r}') \psi(\mathbf{r} + \mathbf{r}') \rangle$, of a critically quenched system behaves like a Bessel function decaying as $C(r) \sim 1/r$, in agreement with the theoretical predictions for the random superposition of waves [10]. For subcritical systems ($\tau > \tau_S$) the network of fluctuations lose correlation and $C(r)$ decays faster. As shown in the following, the early correlations in ψ have a profound effect on the later evolution of the system.

As time proceeds, there is a continuous amplification of ψ until the anharmonic terms of the free energy functional

cannot be neglected and nonlinear dynamics comes into play. While at deep quenches there is a lack of correlation in ψ and the classical picture of SD is recovered, at shallow quenches the early network of density wave fluctuations trigger the inhomogeneous appearance of precursors for crystallization (Fig. 1). Note that the local symmetry of the precursors is dictated by nonlinear dynamic effects and does not necessarily coincide with the symmetry of the phase of equilibrium.

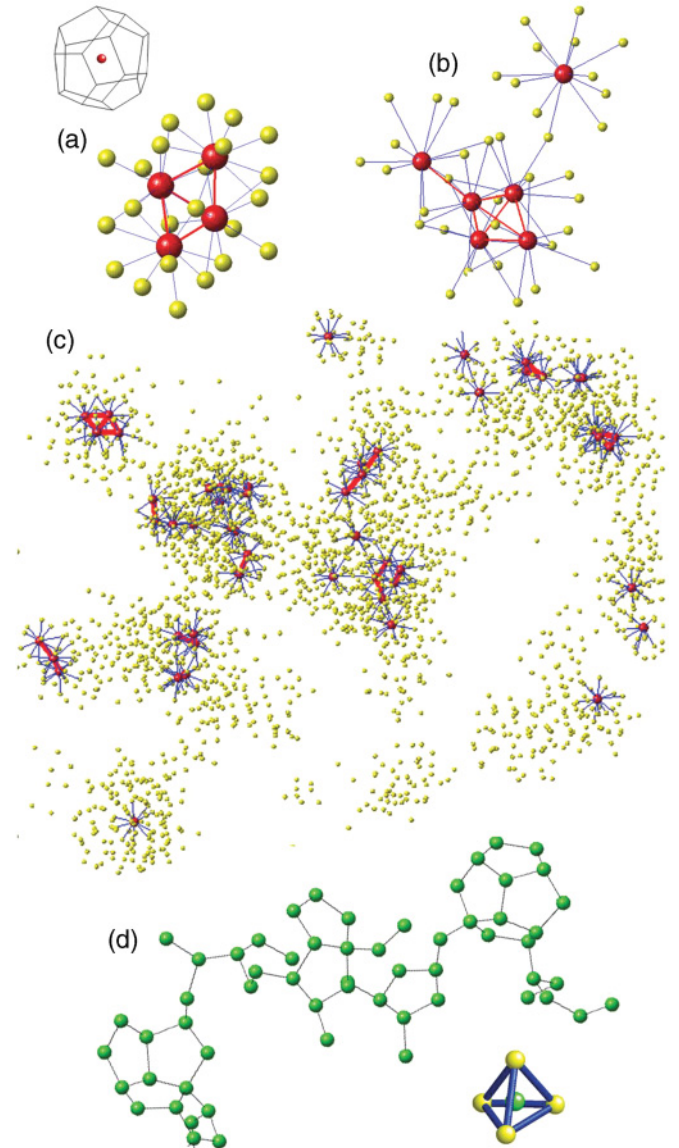


FIG. 2. (Color online) (a) Precursor formed by four icosahedral red (dark gray) particles and their first neighbors in yellow (light gray). Thick red (dark gray) lines indicate bonds between icosahedral particles and thin blue (gray) lines between icosahedra and their first neighbors. Inset: Voronoi diagram of an icosahedral particle (dodecahedron). (b) Precursor formed by a compact cluster of icosahedra arranged in the vertex of a tetrahedron. (c) Propagating amorphous nuclei shown in yellow (light gray) having compact clusters and small chains of icosahedral particles in red (dark gray). (d) Regular tetrahedron (lower right), where yellow spheres (spheres at the vertices) indicate the particles and the green sphere (middle sphere) indicates the tetrahedron's center. Polytetrahedral aggregate (upper), where lines connect tetrahedra with common faces.

In order to track the evolution of the system, we identify structural features by means of Voronoi diagrams through the centers of the particles (with bulk particles defined as local maxima of ψ) that are obtained through conventional approaches [2,3,15]. Voronoi diagrams indicate that the early precursors consist of compact clusters and chains of icosahedrally arranged particles [Figs. 2(a) and 2(b)]. That is, the symmetry of the precursors is dictated by the nonlinear dynamics rather than by equilibrium states.

The presence of precursors with icosahedral symmetry in the early stage of SD is not surprising. One of the oldest scenarios for the formation of amorphous matter and glasses is geometric frustration. According to this scenario, the amorphization of supercooled liquids is related to their tendency to form locally compact structures, like icosahedra, incompatible with translational symmetries [16–19]. The symmetry found in the precursors is also in agreement with the Alexander-McTague prediction, which indicates that local icosahedral order is favored in the absence of an NG mechanism [20–22].

Once the precursors have been formed, they begin to grow with an approximately spherical shape at a constant rate by the addition of new particles [Fig. 2(c)]. Given that the initial symmetry is incompatible with translational order, the aggregation process produces growing amorphous clusters without any appreciable symmetry. As the size of the precursors increases, the geometric frustration is reduced and a number of particles begin to aggregate with a crystalline structure at the front of the propagating precursor [Fig. 3(a)] [23].

This process of surface crystalline nucleation shows similarities with Monte Carlo results for the heterogeneous nucleation on the surface of spherical colloidal seeds [24]. In agreement with the Monte Carlo simulations, here we also observe that the crystalline particles do not span the whole surface of the precursor because crystals cannot grow without generating amorphous regions. Then, the growing nuclei show an amorphous core surrounded by a shell consisting of amorphous and crystalline phases [Fig. 3(a)]. A similar phenomena has been also observed in freezing gold nanoclusters where initially the system crystallizes on the surface of the nuclei while the amorphous core with icosahedrally arranged particles remains stable for some time [25].

Figure 3(b) shows the average radial profile of the ratio between the fraction of crystalline particles on the propagating nuclei, f_{cN} , and the final fraction of crystalline particles throughout the system, f_{cT} . This figure shows that crystal particles begin to nucleate at the surface of the amorphous precursors for radii of the order of $R_c \gtrsim 3a$, with a the interparticle average distance, also in good agreement with the results of Cacciuto *et al.* [24]. Then for $R < R_c$ the high curvature of the precursors clearly frustrates the formation of crystal bonds. The subsequent growth and collision of the different propagating nuclei lead to the formation of a structure having crystalline and amorphous regions [Fig. 3(c)].

Once the SD process has been completed, the volume fraction of crystals in the system depends strongly on temperature. As the depth of quench increases, there is a larger number of unstable modes in the system and $C(r)$ decays faster than $1/r$ (Fig. 1). Consequently, as the temperature of quench drops, the number of amorphous precursors increases, incrementing

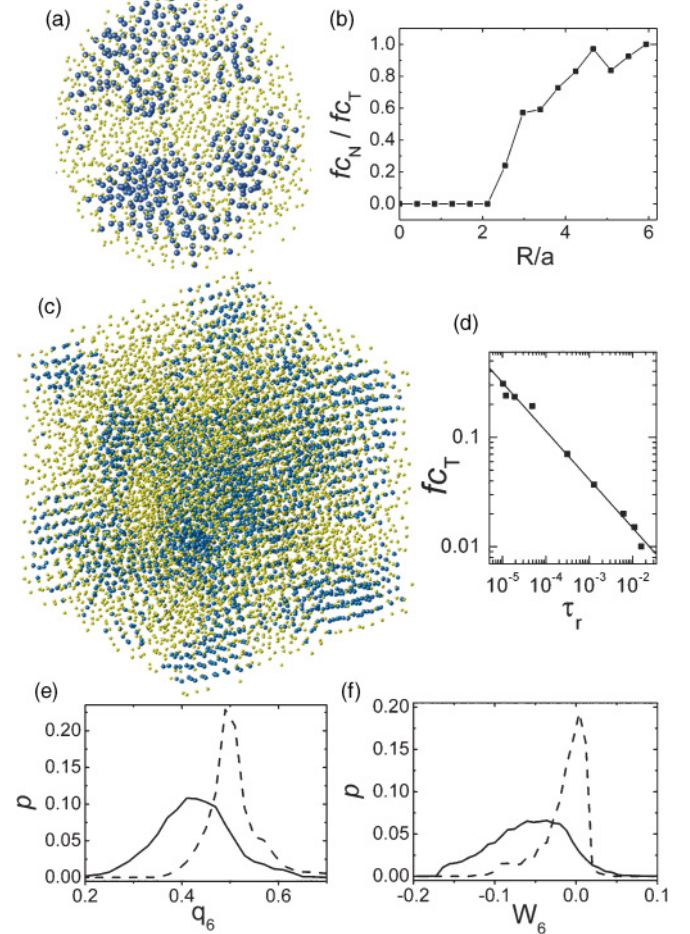


FIG. 3. (Color online) (a) Propagating nucleus formed by an amorphous core shown in small yellow (small light gray) particles and outer crystalline layers shown by big blue (big dark gray) particles. (b) Typical nuclei density profile. (c) System composed of amorphous and crystalline regions after the growth and collision of the different nuclei. (d) Fraction of crystalline particles as a function of τ_r . (e) q_6 , and (f) W_6 distributions for the amorphous (continuous line) and crystalline (dotted line) regions.

in this way the fraction of amorphous material. Figure 3(d) shows the fraction of crystalline particles, f_{cT} , as a function of the reduced temperature $\tau_r = (\tau - \tau_s)/\tau_s$. We found that f_{cT} follows a power law with τ_r ($f_{cT} \sim \tau_r^{-1/2}$). This behavior is consistent with previous results indicating that the average distance between precursors ξ diverge as $\xi \sim \tau_r^{-\eta}$ ($\eta \sim 1/5$, $f_{cT} \sim \xi^3$) [10].

To identify the symmetry of the crystalline phase surrounding the amorphous precursor, we applied the bond order parameter analysis introduced by Steinhardt *et al.* [17], where the local structure is characterized in terms of the symmetry of near-neighbor bonds by using spherical harmonics. The order parameters are calculated by the expressions

$$q_l(i) = \left[\frac{4\pi}{2l+1} \sum_{-l}^l |q_{lm}(i)|^2 \right]^{1/2},$$

$$w_l(i) = \sum_{m_1, m_2, m_3} \begin{pmatrix} l & l & l \\ m_1 & m_2 & m_3 \end{pmatrix} \mathbf{q}_{lm_1}(i) \mathbf{q}_{lm_2}(i) \mathbf{q}_{lm_3}(i),$$

where $(\begin{smallmatrix} l & l & l \\ m_1 & m_2 & m_3 \end{smallmatrix})$ is the $3j$ -Wigner symbol. The vector order parameter is given by

$$\mathbf{q}_{lm}(i) = \frac{1}{cNb(i)} \sum_{j=1}^{Nb(i)} Y_{lm}(\bar{\mathbf{r}}_{ij}),$$

where $\bar{\mathbf{r}}_{ij}$ is the direction of the bond between the i particle and its near neighbor j , $Nb(i)$ is the number of near neighbors of the i particle, $Y_{lm}(\bar{\mathbf{r}}_{ij})$ are the spherical harmonics, and c is a normalization factor such that $\sum_m \mathbf{q}_{lm}(i) \mathbf{q}_{lm}(i)^* = 1$.

The distributions of the bond order parameters are very sensitive to the underlying symmetry, allowing a clear identification of the structure. Figures 3(e) and 3(f) show the distributions of the rotational invariants q_6 and W_6 , for the amorphous and crystalline regions. These distributions reveal that crystal particles arrange in a bcc lattice (peaks at $q_6 \sim 0.5$ and $W_6 \sim 10^{-3}$) while in the amorphous phase both distributions become broader and shifted toward the low bond order parameter region [4,17].

At long times the relaxation of the system continues through a complex process involving structural changes (coarsening), where there is an invasion of the crystalline structure on the amorphous regions. However, at low temperatures the dynamics can be highly arrested and the structure freezes.

In order to study the glasslike amorphous structure in the deep spinodal region, here we also analyze the structural features of a system where the formation of crystals is totally frustrated ($\tau_r > 10^{-2}$ in Fig. 3). Figure 4 shows the pair correlation function $g(r) = \frac{V}{N^2} \langle \sum_i \sum_{j \neq i} \delta(\mathbf{r} - \mathbf{r}_{ij}) \rangle$, where V is the volume and N the number of constituents, for a typical amorphous structure. In this figure we also include the pair correlation function associated with those particles with icosahedral symmetry. Note that the amplitude of the first maximum of the pair correlation function calculated with the

icosahedra is about three times larger than the amplitude of the first maximum of $g(r)$ calculated with all particles. In addition, the position of the first maximum for the icosahedral pair correlation function is slightly smaller than that corresponding to all particles, indicating that the icosahedral bonds are under compression.

The structural features found here (small clusters and chains of icosahedra and the behavior of pair correlation functions) agree with experimental findings in supercooled colloidal systems undergoing NG [4,26], suggesting that icosahedra could also play a role in the amorphization of those systems.

The structural characterization of amorphous matter has been one of the major problems in condensed matter physics during the last 50 years. In this sense, one of the best geometric descriptions is based on aggregates of polytetrahedral clusters that have been invoked in order to describe the structure of liquids, glasses, and quasicrystals.

The geometric features of the tetrahedra can be obtained through Voronoi diagrams [Fig. 2(d)]. To test for the regularity of tetrahedral configurations in the amorphous phase, we calculate the q_3 order parameter, which is sensitive to local tetrahedral order around the tetrahedrons center ($q_3 = \sqrt{5}/3$ for a regular tetrahedron). The left inset of Fig. 4 shows the q_3 distribution for our system. The sharp peak of the distribution at $q_3 \sim 0.73$ clearly indicates that regular tetrahedra are the fundamental units of the amorphous states obtained via SD. The analysis of the tetrahedral configurations also shows that most of the particles ($\sim 90\%$) are involved in at least one regular tetrahedron, indicating the presence of an amorphous phase characterized by a dense polytetrahedral structure [27].

The right inset of Fig. 4 shows a pair correlation function calculated through the centers of the tetrahedra. After a few oscillations, $g(r)$ rapidly decays toward the asymptotic value for $r \gtrsim a$, showing that the tetrahedra aggregate in local configurations without long-range order. By using real space plots we observe configurations of tetrahedra packed on common faces, forming disordered clusters [Fig. 2(d)]. In a manner similar to the dense disordered packing of hard spheres, here we also found that the aggregates are mainly formed by five-fold rings obtained by packing five tetrahedra around a common edge [27].

IV. CONCLUSIONS

We have presented evidence of a mechanism of crystallization during SD that is induced by amorphous precursors. Local icosahedral clusters and amorphous precursors are kinetically favored by the early dynamics of SD. Crystalline particles aggregate on these precursors in a way similar to heterogeneous nucleation on spherical colloidal seeds. Our results are in qualitative agreement with recent NG work in colloidal systems [28]. Although the relaxational mechanism studied here can be easily confused with conventional NG, it is hoped that the phenomenon of crystallization in the neighborhood of the spinodal can be experimentally observed in systems with slow dynamics and a high length-scale selectivity such as hard-sphere colloidal suspensions or block copolymers.

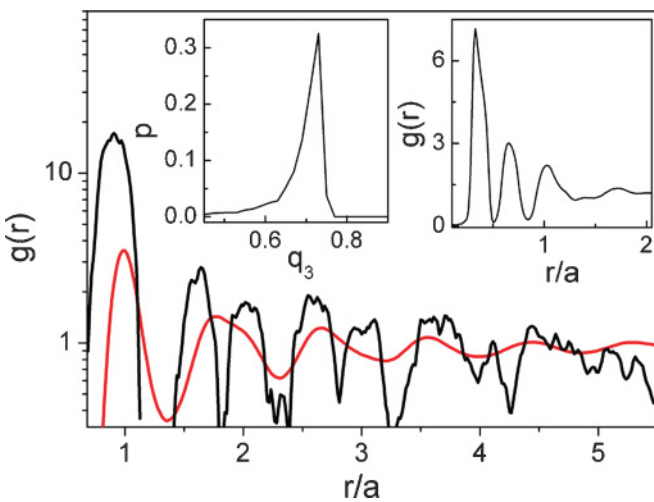


FIG. 4. (Color online) The red (gray) line shows the pair correlation function $g(r)$ calculated by using the centers of all the particles and the black line shows $g(r)$ calculated by only using the centers of the icosahedra. Inset: Distribution for the q_3 bond order parameter (left) and $g(r)$ calculated through the center of the regular tetrahedra (right).

ACKNOWLEDGMENTS

We thank V. Vitelli for helpful discussions and acknowledge support from the Universidad Nacional del Sur (UNS), the

National Research Council of Argentina (CONICET), the National Agency of Scientific and Technique Promotion (AN-PCyT), and the FOM-Shell Industrial Partnership Programme.

-
- [1] P. G. Debenedetti, *Metastable Liquids: Concepts and Principles* (Princeton University Press, Princeton, NJ, 1998).
- [2] D. A. Vega *et al.*, *Phys. Rev. E* **71**, 061803 (2005).
- [3] L. R. Gómez, E. M. Vallés, and D. A. Vega, *Phys. Rev. Lett.* **97**, 188302 (2006).
- [4] U. Gasser *et al.*, *Science* **292**, 258 (2001).
- [5] P. R. ten Wolde, M. J. Ruiz-Montero, and D. Frenkel, *Phys. Rev. Lett.* **75**, 2714 (1995).
- [6] P. R. ten Wolde and D. Frenkel, *Science* **277**, 1975 (1997).
- [7] H. J. Schope, G. Bryant, and W. van Meegen, *Phys. Rev. Lett.* **96**, 175701 (2006).
- [8] P. G. Vekilov, *Cryst. Growth Des.* **4**, 671 (2004).
- [9] J. F. Lutsko and G. Nicolis, *Phys. Rev. Lett.* **96**, 046102 (2006).
- [10] D. A. Vega and L. R. Gómez, *Phys. Rev. E* **79**, 051607 (2009).
- [11] S. Pickering and I. Snook, *Physica A* **240**, 297 (1997).
- [12] M. Seul and D. Andelman, *Science* **267**, 476 (1995).
- [13] W. Li *et al.*, *Macromolecules* **43**, 1644 (2010).
- [14] J. W. Cahn and J. E. Hilliard, *J. Chem. Phys.* **31**, 688 (1959).
- [15] J. C. Crocker and D. G. Grier, *J. Colloid Interface Sci.* **179**, 298 (1996).
- [16] F. C. Frank, *Proc. R. Soc. London Ser. A* **215**, 43 (1952).
- [17] P. J. Steinhardt, D. R. Nelson, and M. Ronchetti, *Phys. Rev. B* **28**, 784 (1983).
- [18] T. Schenk *et al.*, *Phys. Rev. Lett.* **89**, 075507 (2002).
- [19] C. P. Royall *et al.*, *Nature Mater.* **7**, 556 (2008).
- [20] S. Alexander and J. McTague, *Phys. Rev. Lett.* **41**, 702 (1978).
- [21] P. M. Chaikin and T. C. Lubensky, *Principles of Condensed Matter Physics* (Cambridge University Press, Cambridge, 1995).
- [22] C. Ortix, J. Lorenzana, and C. Di Castro, *Phys. Rev. Lett.* **100**, 246402 (2008).
- [23] Here crystalline particles are identified by using an algorithm that finds ordered regions independently of the symmetry.
- [24] A. Cacciuto, S. Auer, and D. Frenkel, *Nature (London)* **428**, 404 (2004).
- [25] H. S. Nam *et al.*, *Phys. Rev. Lett.* **89**, 275502 (2002).
- [26] U. Gasser, A. Schofield, and D. A. Weitz, *J. Phys.: Condens. Matter* **15**, S375 (2003).
- [27] A. V. Anikeenko and N. N. Medvedev, *Phys. Rev. Lett.* **98**, 235504 (2007).
- [28] T. Kawasaki and H. Tanaka, *Proc. Nat. Acad. Sci. USA* **107**, 14036 (2010).